Atmos. Chem. Phys., 14, 1–9, 2014
www.atmos-chem-phys.net/14/1/2014/
doi:10.5194/acp-14-1-2014

Atmospheric Chemistry and Physics Open Access

Chemical feedback effects on the spatial patterns of the NO_x weekend effect: a sensitivity analysis

L. C. Valin[1,*], A. R. Russell[1,], and R. C. Cohen[1,2]**

[1]College of Chemistry, University of California Berkeley, Berkeley, CA 94720, USA
[2]Department of Earth and Planetary Sciences, University of California Berkeley, Berkeley, CA 94720, USA
[*]now at: Lamont-Doherty Earth Observatory, Columbia University, Palisades, NY 10964, USA
[**]now at: Sonoma Technology, Inc., Petaluma, CA 94954, USA

Correspondence to: R. C. Cohen (rccohen@berkeley.edu)

Received: 17 April 2013 – Published in Atmos. Chem. Phys. Discuss.: 19 July 2013
Revised: 18 November 2013 – Accepted: 27 November 2013 – Published: 2 January 2014

Abstract. We examine spatial variations in the weekday–weekend pattern of NO_2 over the Los Angeles metropolitan area using the Ozone Monitoring Instrument (OMI) and then compare the observations to calculations using the WRF-Chem model. We find that the spatial pattern of the weekday–weekend variations of the NO_2 column in the model is significantly different than observed. A sensitivity study shows that the contrasting spatial pattern of NO_2 on weekdays and weekends is a useful diagnostic of emissions and chemistry. These improvements suggest that constraints from space-based observations of the processes affecting urban photochemistry (e.g., spatial patterns of emissions, ratios of VOC to NO_x emissions, rate constants) are possible at a level of detail not previously described.

1 Introduction

In the troposphere, NO_x ($NO+NO_2$) affects ozone production rates, aerosol formation and the oxidative capacity of the atmosphere. NO_x is emitted to the troposphere by fossil-fuel combustion, biomass burning, soil microbial processes, and lightning. During the daytime NO_x is removed from the atmosphere by reactions of HO_x ($OH + HO_2 + RO_2$) with NO_x, primarily by reaction of OH with NO_2 to form nitric acid, $RC(O)O_2$ with NO_2 to form acylperoxy nitrates, and RO_2 with NO to form alkyl nitrates. As a result, the chemical removal of NO_x depends on the concentration of OH and the local mix of volatile organic compound (VOC) precursors to $RC(O)O_2$ and RO_2 (e.g., Browne and Cohen, 2012). Both OH and RO_2 depend non-linearly on NO_x introducing a powerful nonlinear feedback of NO_x on its own lifetime (Fig. 1).

Satellite-based observation of the NO_2 column has provided a wealth of information on NO_x at local (e.g., Bertram et al., 2005; Boersma et al., 2009; Russell et al., 2012), regional (e.g., Richter et al., 2005; Kim et al., 2009; Hudman et al., 2010), and global scales (e.g., Stavrakou et al., 2008; Lamsal et al., 2011), proving particularly useful for study of seasonal (Jaeglé et al., 2005; van der A et al., 2006), interannual (e.g., Richter et al., 2005; van der A et al., 2008; Russell et al., 2012), and weekday–weekend (e.g., Beirle et al., 2003; Kaynak et al., 2009; Russell et al., 2010) trends in NO_2 column. Typically, the observed columns and their trends are used to assess differences in NO_x emissions (e.g., Beirle et al., 2003; Kim et al., 2006). In situ observations (e.g., Thornton et al., 2002; Murhpy et al., 2007) have provided extensive information on the mechanistic details affecting the NO_x lifetime on weekdays and weekends, but lack the coverage in space and time of space-based measurements. With a nadir footprint of 13 km × 24 km and daily, global coverage, the Ozone Monitoring Instrument (OMI – Levelt et al., 2006) provides coverage and spatial detail at a scale relevant to boundary layer NO_x removal (∼10 km–50 km; e.g., Ryerson et al., 2001; Dillon et al., 2002; Beirle et al., 2011; Valin et al., 2011a, b). Recently, OMI observations have been shown to be sensitive not only to NO_x emissions, but also to provide constraints on the NO_x lifetime (e.g., Beirle et al., 2011) and its variation with wind speed (e.g., Valin et al. 2013).

Here, we use OMI observations to describe the spatial variation of the NO_2 column over Los Angeles on weekends and

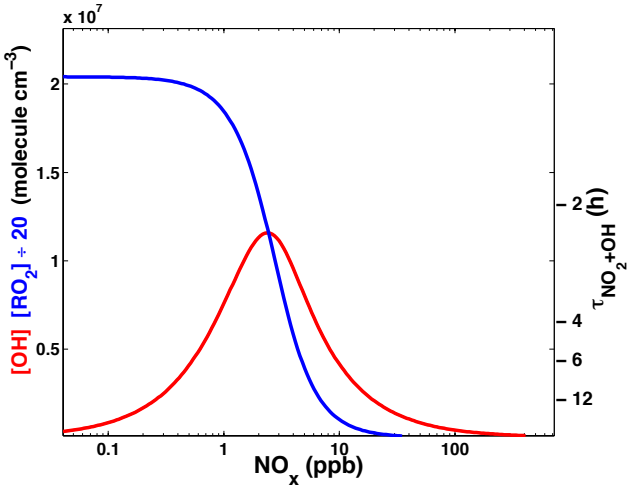

Fig. 1. The steady-state relationship of OH (red) and RO_2 (÷ 20; blue) concentrations to the concentration NO_x using the relationship derived in Murphy et al. (2007) under conditions typical of a polluted summertime urban environment. The lifetime of NO_x with respect to reaction of NO_2 with OH is indicated on the right axis.

weekdays. We then use a series of WRF-Chem model simulations in a sensitivity study to characterize the information contained in the weekday–weekend patterns. From the range of simulations computed, we identify modifications to the base model that produce improved matches to the spatial pattern OMI observations and use this to guide our understanding of the chemical processes that control the NO_2 column.

2 Observations

The Ozone Monitoring Instrument (OMI), a UV/VIS spectrometer developed at KNMI in the Netherlands (Levelt et al., 2006), is mounted on the polar-orbiting, sun-synchronous NASA Aura satellite (Schoerbl et al., 2006). OMI has a 114° field of view, with 480 detector elements devoted to spatial coverage that are averaged onboard to provide 60 pixels across a 2600 km swath of the Earth, and a 2 second integration period that results in a 13 km pixel dimension in the direction of the spacecraft motion. The resulting spatial footprint is as small as 13 km × 24 km. Aura/OMI orbits the Earth over 14 times a day, providing near global coverage at approximately 1:15 p.m. local solar time. Due to the non-overlapping orbital pattern, we oversample the native footprint of OMI (13 km × 24 km at nadir) to achieve a spatial resolution of approximately 10 km × 10 km for temporally averaged fields (e.g., Russell et al., 2010).

Several different analyses of the spectrum measured by OMI are publically available (Bucsela et al., 2006; Boersma et al., 2007; Zhou et al., 2009; Russell et al., 2011). Here, we use the BErkeley High Resolution

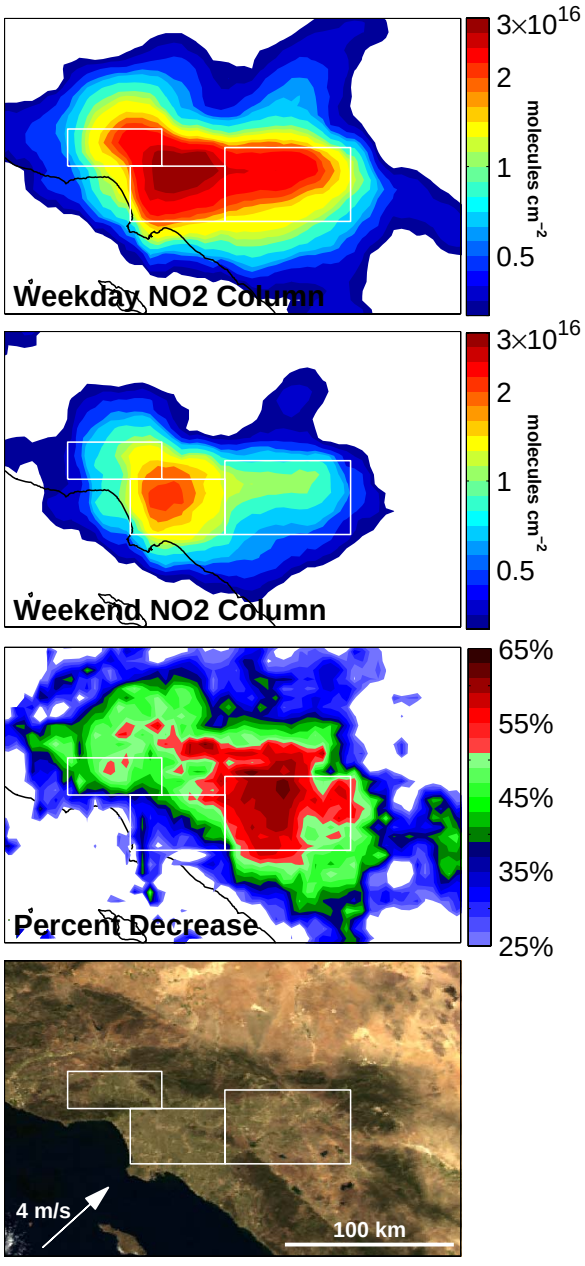

Fig. 2. May–July, 2005–2007 average BEHR NO_2 column (molecules cm^{-2}) for weekdays (top panel) and weekends (second panel), and the percent weekend decrease (third panel). MODIS RGB image of Southern California (fourth panel) with the average North American Regional Reanalysis winds for the region (33.7°–34.0° N; 117.7°–118.4° W) reported in the bottom-left corner, and rectangles marking the San Fernando (NW), Los Angeles (SW) and San Bernardino (E) basins.

(BEHR) retrieval of OMI NO_2 vertical tropospheric columns (available at http://behr.cchem.berkeley.edu; Russell et al., 2011, 2012). Briefly, BEHR derives tropospheric vertical NO_2 column from the NASA standard tropospheric slant

column (Bucsela et al., 2006) using high spatial resolution inputs to the Standard Product AMF lookup table, specifically $12 \times 12\,km^2$ monthly-averaged vertical NO_2 profiles, $0.05° \times 0.05°$ 16-day average MODIS albedo product (MCD43C3), and the Global Land One-kilometer Base Elevation (GLOBE) digital elevation model. Here, we use BEHR version 1.0B. The version number corresponds to the Standard Product version used to derive BEHR, and the version letter corresponds to the version of BEHR for a given Standard Product version.

Figure 2 shows the average May–July, 2005–2007 weekday NO_2 column (Monday–Friday), the weekend column (Saturday–Sunday), and the pattern of weekend NO_2 column decreases in percentage observed by OMI over Southern California. We include a true-color Aqua-MODIS image of the region observed on a cloud-free day (29 May 2005). The Greater Los Angeles metropolitan area consists of three distinct basins: the Los Angeles Basin at the coast (33.8°–34.1° N, 117.8°–118.4° W), the San Fernando Valley to the northwest (34.1°–34.3° N, 118.2°–118.8° W), and the San Bernardino Valley to the east (33.8°–34.2° N, 117.0°–117.8° W). During the summer, the typical daytime meteorology consists of onshore flow entering the Los Angeles Basin at the coast flowing out through the San Bernardino Valley to the east and the San Fernando Valley to the northwest.

Due to the onshore flow and large coastal emission sources, the May–July, 2005–2007 average weekday NO_2 column increases sharply at the coastline to a regional maximum of 3.9×10^{16} molecules cm^{-2} directly over downtown Los Angeles (Fig. 2, top panel). To the east, NO_2 columns decrease gradually through the San Bernardino Valley. To the northwest, in the San Fernando Valley, decreases are sharper than in San Bernardino. On weekends, the average airflow is identical to that on weekdays, but the weekend NO_2 column is markedly lower than the weekday column and the gradients downwind of central Los Angeles are much steeper. Weekend decreases in the NO_2 column are only 25–40 % over coastal and downtown Los Angeles, but are 45–55 % over the San Fernando Valley and an even larger 55–65 % over the San Bernardino Valley.

Large weekend decreases in the NO_2 column and surface concentration have been reported previously using satellite and in situ observations (e.g., Beirle et al., 2003; Murphy et al., 2007; Russell et al., 2010). The changes have been attributed primarily to a weekday–weekend pattern of emissions, with decreases in the US associated with a reduction in freight transport by heavy-duty diesel-powered vehicles (Harley et al., 2005). However, these decreases in emissions result in decreases in NO_x concentrations that affect the NO_x lifetime through the chemical feedbacks on OH and O_3 (e.g., Valin et al., 2011b; Stephens et al., 2008; Pollack et al., 2012; Pusede and Cohen, 2012 and references therein). Previously, analyses have largely assumed that the changes associated with emissions and chemical feedbacks are uniform across an urban center (Beirle et al., 2003; Brioude et al., 2013). The observation that the NO_2 decreases are not spatially uniform has not, to our knowledge, been previously reported or evaluated in a model. In the following, we simulate the weekday–weekend pattern of NO_2 column using WRF-Chem and compare the results to the observations in an effort to understand which model parameters are important for describing the weekday–weekend patterns in Los Angeles, and by analogy, for describing weekday–weekend patterns of NO_2 in other locations. Our goal is not to produce exact agreement, but rather to illustrate that the spatial pattern of observations contains information that can provide new constraints on our understanding of urban photochemistry and emissions.

3 WRF-Chem calculations

We simulate the NO_2 column at the OMI overpass time (1 p.m.) using WRF-Chem (Grell et al., 2005) at 4 km horizontal resolution over a 288 km (N–S) by 480 km (E–W) domain, centered at 34° N, 118° W. We use 36 vertical layers, 14 of which are in the first 1.5 km. As our base case, we use the Regional Acid Deposition Model 2 (RADM2) chemical mechanism, the 2005 National Emissions Inventory (NEI2005) for anthropogenic emissions and the default online module for biogenic emissions as in Grell et al. (2005). Initial and boundary conditions for meteorology are taken from the North American Regional Reanalysis (NARR) and for chemistry are taken from an idealized profile standard to WRF-Chem.

We simulate the average 1 p.m. NO_2 column for 1–14 June 2008 with NEI2005 anthropogenic emissions (weekday) and the same model with an emission rate of $0.625 \times E_{NO_x-NEI2005}$ (weekend), well within the range of values determined previously (∼30–45 % reduction, Harley et al., 2005; Pollack et al., 2012; Oetjen et al., 2013). The first two days are used as spin-up. For the base case, we run WRF-Chem with standard RADM2 chemistry and spatially and temporally uniform weekend emission reductions. We compare results from this base case calculation to weekday–weekend simulations in which we adjust HO_x production from ozone photolysis ($0.5 \times 1.25 \times 1.5 \times 2\times$), VOC emissions ($0.5 \times 2\times$), VOC–OH rate constants ($0.5 \times 2\times$), the NO_2–OH rate constant ($0.5 \times 2\times$), the timing of weekend emissions (1 h delay, 2 h delay), and the spatial distribution of weekend emissions (weekend $E_{NO_x-\text{San Bernardino}}$ of $0.575\times$ and $0.525 \times E_{NO_x-NEI2005}$, and $E_{NO_x-\text{Los Angeles}}$ of $0.640\times$ and $0.654 \times E_{NO_x-NEI2005}$, for domain-average weekend emission of $0.625 \times E_{NO_x-NEI2005}$).

The results from these simulations and the OMI observations are summarized in Table 1. Table 1 reports the percentage reduction in NO_2 column over the entire Los Angeles plume (defined as the area over which OMI observes weekday NO_2 columns exceeding 2.5×10^{15} molecules cm^{-2} within the domain presented:

Table 1. Summary of observed and simulated weekday–weekend patterns of NO_2 column in Los Angeles. Bold-face entries denote results from simulations shown in Fig. 3.

		Total NO_2 decrease in Los Angeles[a]	Fraction of Los Angeles plume[a] where weekend NO_2 decreases are		
			> 35 %	> 45 %	> 55 %
OMI BEHR		**43.0 %**	**0.55**	**0.31**	**0.10**
WRF simulations					
Base	–	**40.4 %**	**0.72**	**0.25**	**0.00**
J_{O_3}	**2** ×	**43.6 %**	**0.55**	**0.36**	**0.12**
	1.5 ×	42.6 %	0.61	0.36	0.04
	1.25 ×	41.9 %	0.66	0.34	0.01
	0.5 ×	39.2 %	0.79	0.09	0.00
E_{VOC}	**2** ×	**42.4 %**	**0.66**	**0.36**	**0.03**
	0.5 ×	39.4 %	0.74	0.14	0.00
k_{VOC+OH}	**2** ×	40.9 %	0.70	0.28	0.00
	0.5 ×	40.8 %	0.82	0.28	0.00
k_{NO_2+OH}	**2** ×	40.6 %	0.75	0.27	0.00
	0.5 ×	40.2 %	0.68	0.23	0.00
$E_{weekend}$ delay[b]	**2 h**	**44.2 %**	**0.74**	**0.43**	**0.01**
	1 h	42.3 %	0.73	0.37	0.00
$E_{weekend}$ spatial dist.[c]	**0.525** ×	**40.0 %**	**0.70**	**0.23**	**0.01**
	0.575 ×	40.2 %	0.71	0.23	0.00

[a] The Los Angeles plume is determined as the region over which the observed weekday NO_2 column exceeds 2.5×10^{15} molecules cm^{-2} within the domain presented (33.3° N–34.8° N, 116.25° W–119.25° W).
[b] Both weekend E_{NO_x} and E_{VOC} are delayed by 2 h.
[c] $E_{NO_x-S.\ Bernardino}$ is $0.575 \times 0.525 \times E_{NO_x-NEI2005}$, and $E_{NO_x-Los\ Angeles}$ is $0.640 \times 0.654 \times E_{NO_x-NEI2005}$, respectively, for domain-average weekend emission of $0.625 \times E_{NO_x-NEI2005}$.

33.3° N–34.8° N, 116.25° W–119.25° W) and the fraction of the Los Angeles plume with weekend decreases in NO_2 column that exceed 35 %, 45 %, and 55 %.

We find that the simulated NO_2 columns, regardless of model scenario, are biased low where NO_2 is low. To correct this bias we add a regionally uniform background column of 5×10^{14} molecules cm^{-2} to both the weekday and weekend simulations for all model scenarios. A column concentration of 5×10^{14} molecules cm^{-2} corresponds to a concentration of 30 ppt if uniformly distributed through the troposphere (0–10 km) and to 200 ppt if restricted to a 1 km boundary layer. This correction does not significantly impact model results where the NO_2 columns are high, but does alter the simulated spatial patterns at the edges of the plume where NO_2 is low (∼20 % effect where NO_2 columns are 2.5×10^{15} molecules cm^{-2}). We test whether a two-week period of simulation is representative of longer time periods by simulating the base case scenario for three months, and find that the magnitude and pattern of decreases simulated in the two-week scenario are comparable to those of the 3-month scenario, indicating their fidelity in representing the meteorological variability of a longer-term simulation. We also test for memory effects by simulating weekday NO_2 column in two-day periods (3–4 June, 4–5 June, …, 13–14 June) initialized with the model NO_2 column from 16:00 LST on the previous weekday to test whether simulation of 14 consecutive weekend days is biased relative to simulation of two-day weekends within a weekly cycle. We find that the memory effect of weekday emissions on the weekend NO_2 column is small compared to the effects of the other parameters tested.

4 Model results and analysis

In Fig. 3, we compare the observed weekday–weekend pattern of NO_2 column (top row) to that simulated with the base model (second row). Integrated over the entire basin, there is only a 2 % difference between observation and simulation, and both exhibit similar spatial patterns. Locally, however, there are large differences between the simulated and observed NO_2 columns (up to a factor of two). OMI observes much higher NO_2 values on the south and west edges of the plume, and the model predicts much higher values in the outflow regions, namely the southeast and northwest edges of the plume. This discrepancy indicates several possible model or observational biases. For instance, NO_2 may be transported downwind too quickly in the model, the observations may be biased over the coastline (e.g., solar glint reflectance impacts on the NO_2 retrieval), or OMI with its pixels of 13 km × 24 km may be smearing the spatial pattern that is simulated at a model horizontal resolution of 4 km × 4 km even though our average of the OMI data takes advantage

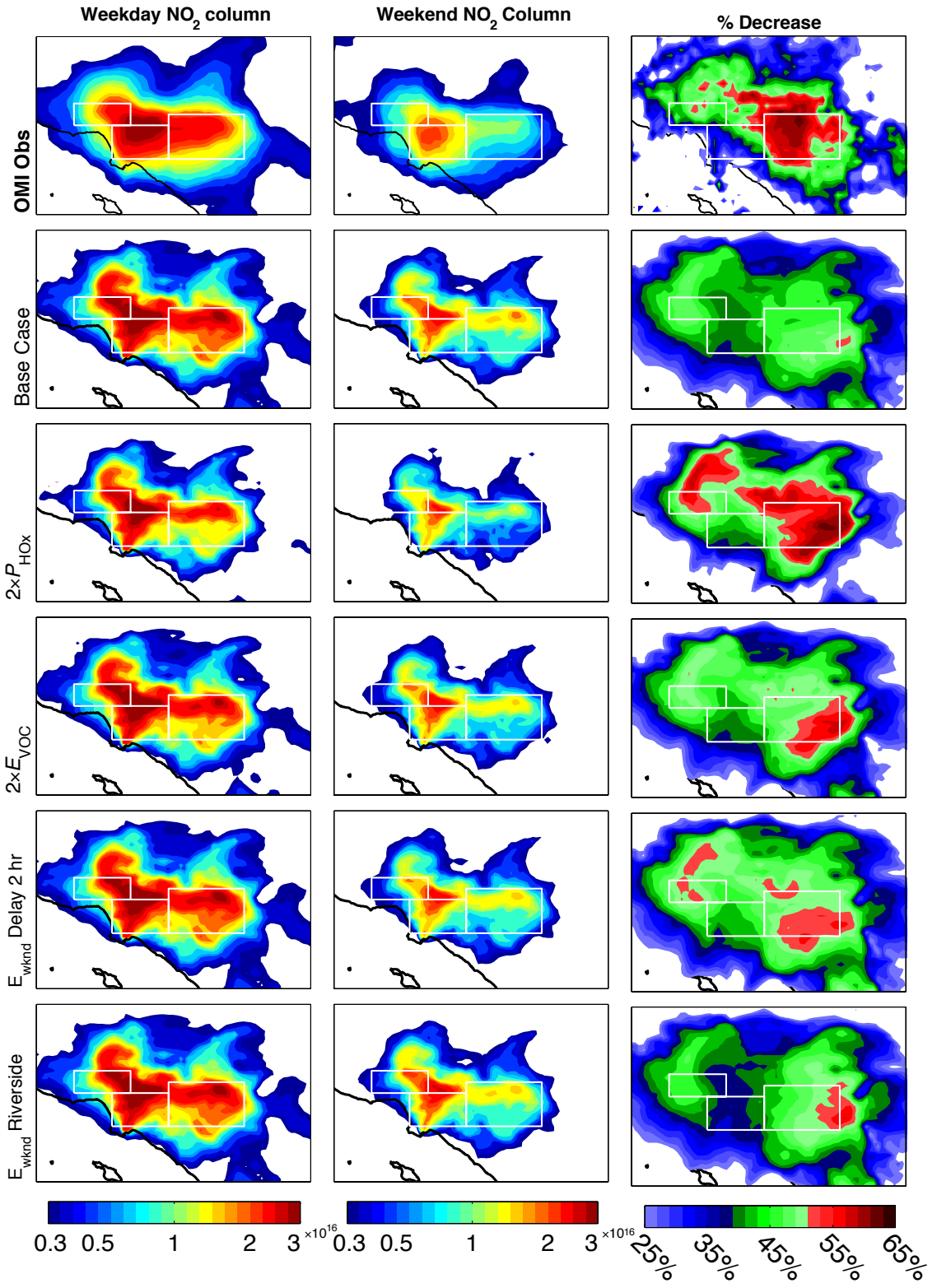

Fig. 3. Weekday NO_2 column (molecules cm^{-2}), weekend NO_2 column (molecules cm^{-2}), and percent change of NO_2 column observed by OMI for May–July 2005–2007 (top row), and simulated with WRF-Chem for 3–14 June 2008 at 13:00 LST using a uniform 37.5 % reduction in NO_x emissions with standard RADM2 chemistry (second row), a 2 × increase of J_{O_3} (third row), a 2 × increase of anthropogenic E_{VOC} (fourth row), a two-hour delay of anthropogenic weekend E_{NO_x} and E_{VOC} relative to weekdays (fifth row), and spatially distinct weekend E_{NO_x} reductions (sixth row; weekend $E_{NO_x-\text{San Bernardino}}$ $0.525 \times E_{NO_x-\text{NEI2005}}$, and $E_{NO_x-\text{Los Angeles}}$ $0.654 \times E_{NO_x-\text{NEI2005}}$, such that the domain-average weekend E_{NO_x} is $0.625 \times E_{NO_x-\text{NEI2005}}$).

of oversampling to increase the resolution to approximately 10 km × 10 km (e.g., Russell et al., 2010).

The large, localized differences between the observed and simulated NO_2 columns highlight the difficulty of accurately computing the interplay of emissions, chemistry and transport or of accounting for the possibility of locally specific observational biases. However, when investigating the patterns of NO_2 column (e.g., weekday–weekend pattern) within self-consistent model simulations or observational data sets, many of these biases are eliminated. OMI, for instance, measures weekday and weekend NO_2 columns that are subject to the same average meteorological patterns and the same average observational biases, and in our WRF-Chem model setup, the weekday and weekend meteorology is identical. As a result, the agreement of simulated and observed NO_2 trends such as the weekday–weekend pattern (Fig. 3 – right column) is more meaningful than the agreement between observations and simulations for a single time period (Fig. 3 – left column). In the base model, simulated NO_2 decreases are too large over the coast (40 % vs. 30 %), are too small over San Bernardino (50 % vs. 60 %), and extend too far inland (150 km vs. 100 km).

The weekday–weekend pattern of the NO_2 column depends both on patterns of NO_x removal and patterns of NO_x emissions. The pattern of removal depends on the relationship of OH and RO_2 concentrations to NO_x (Fig. 1). In Los Angeles, where NO_x concentrations are high (i.e., to the right side of the NO_x–OH curve), a decrease in NO_x emissions on the weekends results in higher concentrations of OH and RO_2. As a result, NO_x is removed faster, and the reduction in NO_2 columns on the weekend is larger than the reduction in NO_x emissions alone. The spatial map of these nonlinear effects reflects the timescale for NO_x removal (Fig. 3 – right column). If the chemical removal of NO_x is slow, the nonlinear decreases will be small over the source where NO_x concentrations are high, but will persist and accumulate far downwind where the concentrations eventually decrease to a value that corresponds to a maximum OH concentration and a minimum in the NO_x chemical lifetime (Fig. 1). If the chemical removal of NO_x is rapid near the source, the nonlinear feedbacks will be large in that location. The discrepancy between the observations and the base simulation (Fig. 3 – first row vs. second row) suggests that the model falls into the first category while the observations fall into the second category, an indication that the simulated OH and RO_2 concentrations are too low (i.e., the model is too far to the right of the NO_2–OH curve presented in Fig. 1).

To test this hypothesis, we evaluate the effects of parameters that influence the concentration of OH and RO_2, and thus affect the timescale of NO_x removal. We double the rate of ozone photolysis to increase the concentration of OH and RO_2 (i.e., shift the entire NO_2–OH curve in Fig. 1 upward). Separately, we double the anthropogenic emissions of VOC to increase the concentration of RO_2 throughout the model domain.

Figure 3 (third row) shows the simulated weekday–weekend pattern of the NO_2 column when HO_x production is increased. Due to the increase in HO_x, the rate of NO_x removal increases, and both weekday and weekend NO_2 columns are smaller than those simulated in the base model. As a result of higher OH and RO_2, the timescale of NO_x losses is shortened compared to the timescale of transport, and, as hypothesized, the weekend decrease is larger near the source and does not extend as far downwind relative to the base case. Here, we adjust HO_x production using ozone photolysis, but other sources of HO_x (or Cl), such as HONO, $ClNO_2$, or CH_2O photolysis may play a role.

Figure 3 (fourth row) shows the simulated weekday–weekend pattern of the NO_2 column when VOC emissions are doubled. VOC both removes OH and leads to OH formation through its feedback on HO_x sources (e.g., O_3, CH_2O). At low NO_x concentrations, the role of VOC as a sink of OH dominates, and OH decreases for any increase in VOC. At high NO_x, however, the role of VOC as a sink of OH is small, and the concentration of OH increases with increases in VOC. As a result, RO_2 increases everywhere for an increase in VOC emissions, and OH increases where NO_x is high (NO_2 column $> 7.5 \times 10^{15}$ molecule cm^{-2}) but decreases where NO_x is low (NO_2 column $< 5 \times 10^{15}$ molecule cm^{-2}). Due to higher OH and RO_2 concentrations over Los Angeles, the timescale of NO_2 removal is shortened when VOC emissions are increased relative to the base model, and the agreement of the simulated weekday–weekend pattern with observations improves. Here, we alter VOC concentrations by altering anthropogenic VOC emissions, but biogenic emissions may also be a significant source of VOC in Los Angeles.

The comparison of modeled and observed weekday–weekend patterns of the NO_2 column suggest that HO_x chemistry in Los Angeles is NO_x-saturated (Fig. 1), but also indicate that the Los Angeles atmosphere is not as far to the right of the NO_x–OH–RO_2 relationship as the model simulation. We find that agreement between model and observation is improved when we increase HO_x production or VOC emissions in the model, but the improvement is similar for both changes (Fig. 3 – third row vs. fourth row). Despite their similarities, there are significant differences between these two adjustments, particularly differences in the relative roles of RO_2 and OH as NO_x sinks (i.e., PAN and $RONO_2$ vs. HNO_3). PAN, for example, is thermally unstable and is much more likely to re-release NO_x downwind than is HNO_3, which is more likely to deposit before undergoing photolysis or reaction with OH. Distinguishing the roles of HNO_3 and PAN chemistry may require more information, such as higher spatial resolution satellite-based measurements at the plume edges where the differences between the two simulations seem the largest, or time-resolved measurements as will become available from geostationary orbit (e.g., GEO-CAPE; Fishman et al., 2008, TEMPO; Chance et al., 2013).

The weekday–weekend pattern of NO_2 columns also depends on weekday–weekend patterns of emissions. The timing of emissions shifts later in the day on weekends (Harley et al., 2005). The delay of emissions on weekends relative to weekdays is expected from a shift in light-duty gasoline vehicle activity later in the day. Weekend emission reductions also vary regionally, and likely locally, due to differing weekday–weekend trends in industry and heavy-duty diesel truck activity relative to passenger vehicle activity (McDonald et al., 2012).

Figure 3 (fifth row) shows the weekday–weekend pattern of NO_2 simulated when we delay the timing of all weekend emissions, both VOC and NO_x, by two hours. When weekend emissions are delayed, the 1 p.m. NO_2 column decreases because the total emissions in the hours prior to the satellite overpass decrease. The timing of emissions affects the magnitude of the observed decreases but does not significantly affect the spatial pattern.

Figure 3 (sixth row) shows the weekday–weekend pattern of NO_2 calculated with a different weekend emission reduction over San Bernardino ($0.525 \times E_{NO_x-NEI2005}$) than over Los Angeles ($0.654 \times E_{NO_x-NEI2005}$), where the total weekend emission reduction is no different than the base case ($0.625 \times E_{NO_x-NEI2005}$). Not surprisingly, the contrast between the East basin (San Bernardino) and the West basin (Los Angeles) is larger when the regional weekday–weekend emission pattern is altered, a modest effect, but one that is consistent with observations that show larger decreases over San Bernardino and smaller decreases over the Los Angeles Basin. This pattern might be used in conjunction with detailed vehicle activity assessments to understand whether the changes are consistent with a differential weekend decrease of heavy-duty diesel truck traffic in the two regions.

In the set of simulations discussed above, we show that the NO_2 column and more specifically weekday–weekend patterns of NO_2 column depend strongly on HO_x production, VOC, and the timing and spatial distribution of weekend emissions. While no single modification provides an unbiased representation of the observed weekday–weekend pattern over Los Angeles, our comparison of the simulated and observed patterns provides a framework for future work aimed at optimally reproducing the weekday–weekend pattern of NO_2 column over Los Angeles or any location. The launch of geosynchronous UV/VIS instruments such as TEMPO (planned for 2018 – Chance et al., 2013) will provide hourly daytime measurements and sampling every 2.5 km × 4.5 km at the surface and a significant increase in the information available to constrain the processes affecting the pattern of weekend NO_2 decreases and the NO_x lifetime.

5 Conclusions

The high spatial resolution of OMI (13 km × 24 km) captures a phenomenal level of detail over the Los Angeles metropolitan area (200 km × 150 km). Comparisons of these observations to a high-resolution model demonstrate that this spatial detail provides information on local patterns of NO_x transport, emissions and chemistry. The observations show that weekend decreases in NO_2 column are smallest over central Los Angeles (25–40 %) where NO_2 columns are high, and are largest downwind of Los Angeles over the San Bernardino and San Fernando valleys (50–65 %).

Using WRF-Chem, we simulate weekday and weekend NO_2 column using a range of model parameters. In the model, the weekend NO_2 column decreases by more than the weekend emissions reduction, a nonlinear feedback that results from the increase in OH concentration and the corresponding decrease in NO_x lifetime that occur when NO_x concentrations are reduced. We show that simulated pattern of weekend NO_2 decreases is sensitive to HO_x production, VOC emissions, and the spatiotemporal distribution of NO_x emissions. The magnitude of the simulated weekday–weekend pattern of column NO_2 is in better agreement with observations when HO_x production is increased, when VOC emissions are increased, or when weekend emissions are delayed or shifted spatially. This is a unique conclusion indicating that satellite measurements of NO_2 can simultaneously teach us about weekday–weekend trends in NO_x emissions and the coupled weekday–weekend variation of the NO_x lifetime.

Further work should focus on the evolution of weekday–weekend NO_2 patterns over time. Its seasonal evolution, for instance, can teach us about chemical feedbacks, as seasonal variations of weekday–weekend emission trends are expected to be small. The interannual evolution, on the other hand, would provide an additional set of constraints on emission trends and the NO_x lifetime.

Acknowledgements. This work was supported by NASA under grant #NNX08AE566, and by NASA Headquarters under the NASA Earth and Space Science Fellowship Program – grant NESSF09.

Edited by: R. Volkamer

References

Beirle, S., Platt, U., Wenig, M., and Wagner, T.: Weekly cycle of NO_2 by GOME measurements: a signature of anthropogenic sources, Atmos. Chem. Phys., 3, 2225-2232, doi:10.5194/acp-3-2225-2003, 2003.

Beirle, S., Boersma, K. F., Platt, U., Lawrence, M. G., and Wagner, T.: Megacity Emissions and Lifetimes of Nitrogen Oxides Probed from Space, Science, 333, 1737–1739, doi:10.1126/science.1207824, 2011.

Bertram, T. H., Heckel, A., Richter, A., Burrows, J. P., and Cohen, R. C.: Satellite measurements of daily variations in soil NO_x emissions, Geophys. Res. Lett., 32, L24812, doi:10.1029/2005GL024640, 2005.

Boersma, K. F., Eskes, H. J., Veefkind, J. P., Brinksma, E. J., van der A, R. J., Sneep, M., van den Oord, G. H. J., Levelt, P. F., Stammes, P., Gleason, J. F., and Bucsela, E. J.: Near-real time retrieval of tropospheric NO_2 from OMI, Atmos. Chem. Phys., 7, 2103–2118, doi:10.5194/acp-7-2103-2007, 2007.

Boersma, K. F., Jacob, D. J., Trainic, M., Rudich, Y., DeSmedt, I., Dirksen, R., and Eskes, H. J.: Validation of urban NO_2 concentrations and their diurnal and seasonal variations observed from the SCIAMACHY and OMI sensors using in situ surface measurements in Israeli cities, Atmos. Chem. Phys., 9, 3867–3879, doi:10.5194/acp-9-3867-2009, 2009.

Brioude, J., Angevine, W. M., Ahmadov, R., Kim, S.-W., Evan, S., McKeen, S. A., Hsie, E.-Y., Frost, G. J., Neuman, J. A., Pollack, I. B., Peischl, J., Ryerson, T. B., Holloway, J., Brown, S. S., Nowak, J. B., Roberts, J. M., Wofsy, S. C., Santoni, G. W., Oda, T., and Trainer, M.: Top-down estimate of surface flux in the Los Angeles Basin using a mesoscale inverse modeling technique: assessing anthropogenic emissions of CO, NO_x and CO_2 and their impacts, Atmos. Chem. Phys., 13, 3661–3677, doi:10.5194/acp-13-3661-2013, 2013.

Browne, E. C. and Cohen, R. C.: Effects of biogenic nitrate chemistry on the NO_x lifetime in remote continental regions, Atmos. Chem. Phys., 12, 11917–11932, doi:10.5194/acp-12-11917-2012, 2012.

Bucsela, E. J., Celarier, E. A., Wenig, M. O., Gleason, J. F., Veefkind, J. P., Boersma, K. F., and Brinksma, E. J.: Algorithm for NO_2 vertical column retrieval from the ozone monitoring instrument, IEEE Trans. Geosci. Remote Sens., 44, 1245–1258, doi:10.1109/tgrs.2005.863715, 2006.

Chance, K., Suleiman, R. M., Flittner, D. E., Al-Saadi, J., Janz, S. J.: Tropospheric emissions: monitoring of pollution (TEMPO), Proc. SPIE 8866, Earth Observing Systems XVIII, 88660D, doi:10.1117/12.2024479, 2013.

Dillon, M. B., Lamanna, M. S., Schade, G. W., Goldstein, A. H., and Cohen, R. C.: Chemical evolution of the Sacramento urban plume: Transport and oxidation, J. Geophys. Res.-Atmos., 107, ACH 3-1–ACH 3-15, doi:10.1029/2001jd000969, 2002.

Fishman, J., Bowman, K. W., Burrows, J. P., Richter, A., Chance, K. V., Edwards, D. P., Martin, R. V., Morris, G. A., Pierce, R. B., Ziemke, J. R., Al-Saadi, J. A., Creilson, J. K., Schaack, T. K., and Thompson, A. M.: Remote sensing of tropospheric pollution from space, Bull. Amer. Meteor. Soc., 89, 805–821, doi:10.1175/2008bams2526.1, 2008.

Grell, G. A., Peckham, S. E., Schmitz, R., McKeen, S. A., Frost, G., Skamarock, W. C., and Eder, B.: Fully coupled "online" chemistry within the WRF model, Atmos. Environ., 39, 6957–6975, doi:10.1016/j.atmosenv.2005.04.027, 2005.

Harley, R. A., Marr, L. C., Lehner, J. K., and Giddings, S. N.: Changes in motor vehicle emissions on diurnal to decadal time scales and effects on atmospheric composition, Environ. Sci. Technol., 39, 5356–5362, doi:10.1021/es048172+, 2005.

Hudman, R. C., Russell, A. R., Valin, L. C., and Cohen, R. C.: Interannual variability in soil nitric oxide emissions over the United States as viewed from space, Atmos. Chem. Phys., 10, 9943–9952, doi:10.5194/acp-10-9943-2010, 2010.

Jaeglé, L., Steinberger, L., Martin, R. V., and Chance, K.: Global partitioning of NO_x sources using satellite observations: Relative roles of fossil fuel combustion, biomass burning and soil emissions, Faraday Discuss., 130, 407–423, doi:10.1039/B502128F, 2005.

Kaynak, B., Hu, Y., Martin, R. V., Sioris, C. E., and Russell, A. G.: Comparison of weekly cycle of NO_2 satellite retrievals and NO_x emission inventories for the continental United States, J. Geophys. Res.-Atmos., 114, D05302, doi:10.1029/2008JD010714, 2009.

Kim, S. W., Heckel, A., McKeen, S. A., Frost, G. J., Hsie, E. Y., Trainer, M. K., Richter, A., Burrows, J. P., Peckham, S. E., and Grell, G. A.: Satellite-observed US power plant NO_x emission reductions and their impact on air quality, Geophys. Res. Lett., 33, 5, L22812, doi:10.1029/2006GL027749, 2006.

Kim, S. W., Heckel, A., Frost, G. J., Richter, A., Gleason, J., Burrows, J. P., McKeen, S., Hsie, E. Y., Granier, C., and Trainer, M.: NO_2 columns in the western United States observed from space and simulated by a regional chemistry model and their implications for NO_x emissions, J. Geophys. Res.-Atmos., 114, 29, D11301, doi:10.1029/2008JD011343, 2009.

Lamsal, L. N., Martin, R. V., Padmanabhan, A., van Donkelaar, A., Zhang, Q., Sioris, C. E., Chance, K., Kurosu, T. P., and Newchurch, M. J.: Application of satellite observations for timely updates to global anthropogenic NO_x emission inventories, Geophys. Res. Lett., 38, doi:10.1029/2010GL046476, 2011.

Levelt, P. F., Van den Oord, G. H. J., Dobber, M. R., Malkki, A., Visser, H., de Vries, J., Stammes, P., Lundell, J. O. V., and Saari, H.: The Ozone Monitoring Instrument, IEEE Trans. Geosci. Remote Sens., 44, 1093–1101, doi:10.1109/tgrs.2006.872333, 2006.

McDonald, B. C., Dallmann, T. R., Martin, E. W., and Harley, R. A.: Long-Term Trends in Nitrogen Oxide Emissions from Motor Vehicles at National, State, and Air Basin Scales, J. Geophys. Res., 117, D00V18, doi:10.1029/2012JD018304, 2012.

Murphy, J. G., Day, D. A., Cleary, P. A., Wooldridge, P. J., Millet, D. B., Goldstein, A. H., and Cohen, R. C.: The weekend effect within and downwind of Sacramento – Part 1: Observations of ozone, nitrogen oxides, and VOC reactivity, Atmos. Chem. Phys., 7, 5327–5339, doi:10.5194/acp-7-5327-2007, 2007.

Oetjen, H., Baidar, S., Krotkov, N. A., Lamsal, L. N., Lechner, M., and Volkamer, R.: Airborne MAX-DOAS measurements over California: Testing the NASA OMI tropospheric NO_2 product, J. Geophys. Res.-Atmos., 118, 7400–7413, doi:10.1002/jgrd.50550, 2013.

Pollack, I. B., Ryerson, T. B., Trainer, M., Parrish, D. D., Andrews, A. E., Atlas, E. L., Blake, D. R., Brown, S. S., Commane, R., Daube, B. C., de Gouw, J. A., Dube, W. P., Flynn, J., Frost, G. J., Gilman, J. B., Grossberg, N., Holloway, J. S., Kofler, J., Kort, E. A., Kuster, W. C., Lang, P. M., Lefer, B., Lueb, R. A., Neuman, J. A., Nowak, J. B., Novelli, P. C., Peischl, J., Perring, A. E., Roberts, J. M., Santoni, G., Schwarz, J. P., Spackman, J. R., Wagner, N. L., Warneke, C., Washenfelder, R. A., Wofsy, S. C., and Xiang, B.: Airborne and ground-based observations of a weekend effect in ozone, precursors, and oxidation products in the California South Coast Air Basin, J. Geophys. Res.-Atmos., 117, D00V05, doi:10.1029/2011jd016772, 2012.

Pusede, S. E. and Cohen, R. C.: On the observed response of ozone to NO_x and VOC reactivity reductions in San Joaquin Valley

California 1995–present, Atmos. Chem. Phys., 12, 8323–8339, doi:10.5194/acp-12-8323-2012, 2012

Richter, A., Burrows, J. P., Nuss, H., Granier, C., and Niemeier, U.: Increase in tropospheric nitrogen dioxide over China observed from space, Nature, 437, 129–132, doi:10.1038/nature04092, 2005.

Russell, A. R., Valin, L. C., Bucsela, E. J., Wenig, M. O., and Cohen, R. C.: Space-based constraints on spatial and temporal patterns of NO_x emissions in California, 2005-2008, Env. Sci. Tech., 44, 3608–3615, doi:10.1021/es903451j, 2010.

Russell, A. R., Perring, A. E., Valin, L. C., Bucsela, E. J., Browne, E. C., Min, K. E., Wooldridge, P. J., and Cohen, R. C.: A high spatial resolution retrieval of NO_2 column densities from OMI: method and evaluation, Atmos. Chem. Phys., 11, 8543–8554, doi:10.5194/acp-11-8543-2011, 2011.

Russell, A. R., Valin, L. C., and Cohen, R. C.: Trends in OMI NO_2 observations over the United States: effects of emission control technology and the economic recession, Atmos. Chem. Phys., 12, 12197–12209, doi:10.5194/acp-12-12197-2012, 2012.

Ryerson, T. B., Trainer, M., Holloway, J. S., Parrish, D. D., Huey, L. G., Sueper, D. T., Frost, G. J., Donnelly, S. G., Schauffler, S., Atlas, E. L., Kuster, W. C., Goldan, P. D., Hubler, G., Meagher, J. F., and Fehsenfeld, F. C.: Observations of ozone formation in power plant plumes and implications for ozone control strategies, Science, 292, 719–723, doi:10.1126/science.1058113, 2001.

Schoeberl, M., Douglass, A., Hilsenrath, E., Bhartia, P., Beer, R., Waters, J., Gunson, M., Froidevaux, L., Gille, J., Barnett, J., Levelt, P., and DeCola, P.: Overview of the EOS Aura Mission, IEEE Trans. Geosci. Remote Sens., 44, 1066–1074, doi:10.1109/tgrs.2005.861950, 2006.

Stavrakou, T., Muller, J. F., Boersma, K. F., De Smedt, I., and van der A, R. J.: Assessing the distribution and growth rates of NO_x emission sources by inverting a 10-year record of NO_2 satellite columns, Geophys. Res. Lett., 35, L10801, doi:10.1029/2008GL033521, 2008.

Stephens, S., Madronich, S., Wu, F., Olson, J. B., Ramos, R., Retama, A., and Munoz, R.: Weekly patterns of Mexico City's surface concentrations of CO, NO_x, PM_{10} and O_3 during 1986–2007, Atmos. Chem. Phys., 8, 5313–5325, doi:10.5194/acp-8-5313-2008, 2008.

Thornton, J. A., Wooldridge, P. J., Cohen, R. C., Martinez, M., Harder, H., Brune, W. H., Williams, E. J., Roberts, J. M., Fehsenfeld, F. C., Hall, S. R., Shetter, R. E., Wert, B. P., and Fried, A.: Ozone production rates as a function of NO_x abundances and HO_x production rates in the Nashville urban plume, J. Geophys. Res.-Atmos., 107, 4146, doi:10.1029/2001JD000932, 2002.

Valin, L., Russell, A., Bucsela, E., Veefkind, J., and Cohen, R.: Observation of slant column NO_2 using the super-zoom mode of AURA-OMI, Atmos. Meas. Tech., 4, 1929–1935, doi:10.5194/amt-4-1929-2011, 2011a.

Valin, L., Russell, A., Hudman, R., and Cohen, R.: Effects of model resolution on the interpretation of satellite NO_2 observations, Atmos. Chem. Phys., 11, 11647–11655, doi:10.5194/acp-11-11647-2011, 2011b.

Valin, L. C., Russell, A. R., and Cohen, R. C.: Variations of OH radical in an urban plume inferred from NO_2 column measurements, Geophys. Res. Lett., 40, 1856–1860, doi:10.1002/grl.50267, 2013.

van der A, R. J., Peters, D., Eskes, H., Boersma, K. F., Van Roozendael, M., De Smedt, I., and Kelder, H. M.: Detection of the trend and seasonal variation in tropospheric NO_2 over China, J. Geophys. Res. – Atmos., 111, D12317, doi:10.1029/2005JD006594, 2006.

van der A, R. J., Eskes, H. J., Boersma, K. F., van Noije, T. P. C., Van Roozendael, M., De Smedt, I., Peters, D., and Meijer, E. W.: Trends, seasonal variability and dominant NO_x source derived from a ten year record of NO_2 measured from space, J. Geophys. Res.-Atmos., 113, D04302, doi:10.1029/2007JD009021, 2008.

Zhou, Y., Brunner, D., Boersma, K. F., Dirksen, R., and Wang, P.: An improved tropospheric NO_2 retrieval for OMI observations in the vicinity of mountainous terrain, Atmos. Meas. Tech., 2, 401–416, doi:10.5194/amt-2-401-2009, 2009.